Inorganic Chemistry

Article

pubs.acs.org/IC

Varying the Electronic Structure of Surface-Bound Ruthenium(II) Polypyridyl Complexes

Dennis L. Ashford, M. Kyle Brennaman, Robert J. Brown, Shahar Keinan, Javier J. Concepcion, John M. Papanikolas, Joseph L. Templeton, and Thomas J. Meyer*

Department of Chemistry, University of North Carolina at Chapel Hill, CB 3290, Chapel Hill, North Carolina 27599, United States

Supporting Information

ABSTRACT: In the design of light-harvesting chromophores for use in dye-sensitized photoelectrosynthesis cells (DSPECs), surface binding to metal oxides in aqueous solutions is often inhibited by synthetic difficulties. We report here a systematic synthesis approach for preparing a family of Ru(II) polypyridyl complexes of the type $[Ru(4,4'\text{-}R_2\text{-}bpy)_2(4,4'\text{-}(PO_3H_2)_2\text{-}bpy)]^{2+}$ (4,4′$(PO_3H_2)_2$-bpy = [2,2′-bipyridine]-4,4′-diylbis(phosphonic acid); 4,4′-R_2-bpy = 4,4′-R_2-2,2′-bipyridine; and R = OCH_3, CH_3, H, or Br). In this series, the nature of the 4,4′-R_2-bpy ligand is modified through the incorporation of electron-donating (R = OCH_3 or CH_3) or electron-withdrawing (R = Br) functionalities to tune redox potentials and excited-state energies. Electrochemical measurements show that the ground-state potentials, $E^{o\prime}(Ru^{3+/2+})$, vary from 1.08 to 1.45 V (vs NHE) when the complexes are immobilized on TiO_2 electrodes in aqueous $HClO_4$ (0.1 M) as a result of increased Ru dπ–π^* back-bonding caused by the lowering of the π^* orbitals on the 4,4′-R_2-bpy ligand. The same ligand variations cause a negligible shift in the metal-to-ligand charge-transfer absorption energies. Emission energies decrease from λ_{max} = 644 to 708 nm across the series. Excited-state redox potentials are derived from single-mode Franck–Condon analyses of room-temperature emission spectra and are discussed in the context of DSPEC applications.

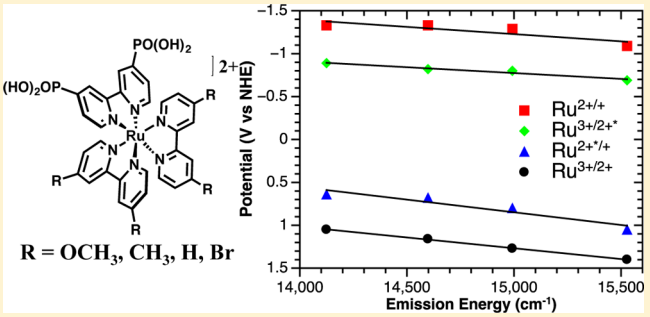

INTRODUCTION

Light absorption throughout the visible and near-IR spectra is required for efficient dye-sensitized solar cells (DSSCs) and dye-sensitized photoelectrosynthesis cells (DSPECs).[1−7] Chromophores suitable to drive water-splitting reactions in DSPEC photoanodes must satisfy four design criteria: (1) surface-binding groups (typically carboxylates or phosphonates), (2) high molar absorptivity throughout the visible and near-IR spectra, (3) an excited-state redox potential that is sufficient to undergo rapid and efficient electron injection into the conduction band of a metal oxide semiconductor (typically anatase TiO_2), and (4) the resulting oxidized chromophore must have the thermodynamic potential sufficient to oxidize an adjacent water-oxidation catalyst to its most active form by electron transfer.[8−11]

Ruthenium polypyridyl complexes have been extensively studied for use as chromophores in DSSCs and DSPECs.[11−15] They typically absorb light in the visible spectrum, have sufficient excited-state potentials to inject electrons into the conduction band of TiO_2, and are capable of driving water oxidation with $E^o \geq 1.23$ V (vs NHE) in appropriately designed complexes.[5,16−18]

We have previously demonstrated stable surface linkages with phosphonate derivatives for a variety of polypyridyl Ru(II) complexes and assemblies.[12,19−22] The extent of this chemistry has been limited by difficulties associated with synthesis. The dearth of these complexes has inhibited studies exploring the role of synthetic changes on the key parameters for photoanode applications, namely, excited- and ground-state redox potentials.[1,10,23−26] We report herein a systematic study of the synthesis of phosphonate-derivatized Ru(II) polypyridyls of the general form $[Ru(4,4'\text{-}R_2\text{-}bpy)_2(4,4'\text{-}(PO_3H_2)_2\text{-}bpy)]^{2+}$ (4,4′$(PO_3H_2)_2$-bpy = [2,2′-bipyridine]-4,4′-diylbis(phosphonic acid), 4,4′-R_2-bpy = 4,4′-R_2-2,2′-bipyridine, and R = OCH_3, CH_3, H, or Br; Figure 1) and their electrochemical, spectroscopic, and excited-state properties.

EXPERIMENTAL SECTION

Materials. Tetraethyl-[2,2′-bipyridine]-4,4′-diylbis(phosphonate),[27] poly-Ru(1,4-cyclooctadiene)Cl_2,[28] and $[Ru(2,2\text{-bipyridine})_2([2,2\text{-bipyridine}]\text{-}4,4\text{-diyldiphosphonic acid})]Cl_2$ (**RuP**)[27] were synthesized as previously reported. Distilled water was further purified using a Milli-Q Ultrapure water purification system. All other reagents were ACS grade and used without further purification. Fluoride-doped tin oxide (FTO)-coated glass (Hartford Glass; sheet resistance = 15 Ω/□) was cut into 10 × 40 mm^2 strips and used as the substrate for ZrO_2 and TiO_2 nanoparticle films. Microwave reactions were carried out using a CEM MARS microwave reactor. A CEM HP-500 Plus

Received: August 26, 2014
Revised: December 2, 2014
Accepted: December 3, 2014
Published: December 23, 2014

DOI: 10.1021/ic501682k
Inorg. Chem. 2015, 54, 460−469

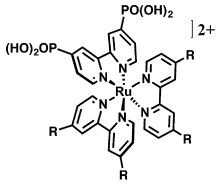

Figure 1. Structures of **RuPOMe**, **RuPMe**, **RuP**, and **RuPBr**.

Teflon-coated microwave vessel (100 mL) was used at a power setting of 400 W. The vessel was rotated and stirred throughout the microwave procedure. The pressure of the reaction vessel was monitored throughout the reaction and never exceeded 300 psi.

Metal-Oxide Films. Nano-TiO_2[29] and nano-ZrO_2[30] films, typically 5−7 μm thick with a coating area of roughly 10 × 15 mm^2, were prepared according to the literature. Dye-absorption isotherms on TiO_2 (Figure S2) were obtained by soaking the films in methanol solutions of [Ru(4,4′-dimethoxy-2,2′-bipyridine)$_2$([2,2′-bipyridine]-4,4′-diyldiphosphonic acid)]Cl_2 (**RuPOMe**), [Ru(4,4-dimethyl-2,2-bipyridine)$_2$([2,2-bipyridine]-4,4-diyldiphosphonic acid)]Cl_2 (**RuPMe**), and [Ru(4,4′-dibromo-2,2′-bipyridine)$_2$([2,2′-bipyridine]-4,4′-diyldiphosphonic acid)]Cl_2 (**RuPBr**) at concentrations of 10, 20, 50, 100, 150, and 200 μM. The slides were then removed, rinsed with methanol, and dried over a stream of nitrogen.

UV−Visible Absorption Spectra. UV−visible absorption spectra were obtained by placing the dry derivatized films perpendicular to the detection beam path of a UV−vis-NIR absorption dual-beam spectrophotometer (HP 8453A). The expression $\Gamma = A(\lambda)/(\varepsilon(\lambda) \times 1000)$ was used to calculate surface coverage (Γ) on metal-oxide electrodes where A is the absorption and $\varepsilon(\lambda)$ is the molar absorptivity at wavelength λ.[31] Maximum surface coverage (Γ_{max}) and surface-binding constants (K_{ad}) on TiO_2 for **RuPOMe**, **RuPMe**, and **RuPBr** were obtained by evaluation of the Langmuir isotherm (eq 1) with [X] the concentration of the complex in the loading solutions (Figure S2).[32] All subsequent measurements were carried out on films loaded from solutions of a ruthenium complex in methanol (100 μM), which yielded surface coverages of ∼7 × 10^{-8} mol cm^{-2}.

$$\Gamma = \frac{\Gamma_{max} K_{ad}[X]}{1 + K_{ad}[X]} \quad (1)$$

Steady-State and Time-Resolved Emission. Measurements were carried out by inserting derivatized thin films of ZrO_2 at a 45° angle into a standard 1 cm path length cuvette containing aqueous $HClO_4$ (0.1 M). Emission spectra were collected at room temperature using an Edinburgh FLS920 spectrometer with luminescence first passing through a 495 nm long-pass color filter, then a single-grating (1800 L/mm, 500 nm blaze) Czerny−Turner monochromator (5 nm bandwidth), and finally detected by a Peltier-cooled Hamamatsu R2658P photomultiplier tube. For steady-state experiments, samples were excited using light output from a combination of a housed 450 W Xe lamp and a single-grating (1800 L/mm, 250 nm blaze) Czerny−Turner monochromator with 5 nm bandwidth. The dynamics of emission decay were monitored using the FLS920 time-correlated single-photon-counting capability (1024 channels; 1 ns per channel) with each data set collecting >5000 counts in the maximum channel. Excitation was provided by an Edinburgh EPL-445 ps pulsed-diode laser (444.2 nm, 80 ps fwhm) operated at 200 kHz. Kinetics were evaluated using either Edinburgh or Origin software.

Electrochemical Measurements. Measurements were carried out with a CH Instruments 660D potentiostat with a Pt-wire counter electrode and either a $Ag/AgNO_3$ (0.01 M $AgNO_3$/0.1 M tetra-*n*-butylammonium hexafluorophosphate ($TBAPF_6$) CH_3CN; −0.09 V vs $Fc^{0/+}$) or a Ag/AgCl (3 M NaCl; 0.198 V vs NHE) reference electrode. $E^{o'}$ values were obtained from the peak currents in square-wave voltammograms. Reductive electrochemistry was conducted with complexes dissolved in 80:20 CH_3CN/H_2O ([complex] = 1 mM) deaerated with argon for 5 min with a glassy-carbon working electrode, a Pt-wire counter, and a $Ag/AgNO_3$ reference. Surface electrochemistry was conducted by immersing derivatized TiO_2 working electrodes in aqueous $HClO_4$ (0.1 M).[19,21,27]

Computational Methods. All molecular geometries were calculated by density functional theory (DFT) with the B3LYP[33,34] functional and the LanL2DZ[35,36] basis set. Solvent-environment effects were described by using the polarizable continuum model (PCM), using the integral equation formalism variant for water. To ensure finding the exact geometrical minima, tighter convergence criteria and a more accurate numerical-integration grid were specified. Frequencies were calculated and checked to make sure that all frequencies were positive. Electronic spectra were calculated using time-dependent (TD) DFT, on the basis of the procedure previously outlined by Jacquemin et al.[37,38] The geometry-optimized structures were used in the TD DFT calculations, using the PBE0[39,40] functional and the same basis set and solvent effects as in the geometry optimization. The adiabatic approximation of TD DFT was used to solve for 100 singlet excited states.[41] To prevent spurious effects caused by charge localization, the total charge on the molecule was set to zero by removing two protons from the structure, one from each PO_3H_2 group. All calculations were conducted in Gaussian 09, Revision C.01.[42]

SYNTHESIS OF LIGANDS AND COMPLEXES

4,4′-Dibromo-2,2′-bipyridine. 4,4′-Dimethoxy-2,2′-bipyridine (2.7 g, 12.5 mmol) was dissolved in PBr_3 (20 mL, 212 mmol) under an atmosphere of argon. The reaction mixture was heated to 180 °C with vigorous stirring. The reaction was completed in 3 h and followed by TLC. After cooling the reaction to room temperature, crushed ice was carefully added, followed by the addition of concentrated aqueous ammonia alternated with the addition of ice. (***Caution!*** *Addition of ice and ammonia causes the mixture to heat quickly; take great care when adding them alternately to the PBr_3 solution.*) Enough ammonia was added to reach a pH of ∼10, at which point a significant amount of precipitate formed. The solution was then transferred to a separatory funnel and extracted with ether (4 × 70 mL). The organic layers were combined, dried over $MgSO_4$, filtered, and the solvent was removed by rotary evaporation. A white solid (1.81 g, 47%) was isolated. The solid appeared clean via ^{1}H NMR but contained a small phosphorus impurity. The impurity was removed by running the sample through a plug of silica with dichloromethane as the eluent. The characterization matches that previously reported.[43] ^{1}H NMR (400 MHz, $CDCl_3$): δ (ppm) 8.59 (d, 2H), 8.465 (d, 2H), 7.49 (dd, 2H).

[2,2′-Bipyridine]-4,4′-diyldiphosphonic Acid. Tetraethyl [2,2′-bipyridine]-4,4′-diylbis(phosphonate) (1.0 g, 2.33 mmol) was dissolved in anhydrous CH_2Cl_2 (∼50 mL) under an atmosphere of argon. To the solution was added bromotrimethylsilane (2.15 mL, 12.1 mmol), and the reaction was stirred at room temperature under an atmosphere of argon for 3 days. The solvent was removed under vacuum, and anhydrous methanol (∼30 mL) was added. The solution was stirred for 30 min at room temperature, the methanol was removed under vacuum, and ether (∼60 mL) was added to the white solid. The suspension was stirred for 2 h, and the white solid was collected by suction filtration. This compound was used without further purification (0.74 g, 87%). ^{1}H NMR (400 MHz, d_6-DMSO): δ (ppm) 8.85 (t, 2 H), 8.66 (d, 2 H), 7.75 (dd, 2H).

General Procedure for Ru(4,4′-R_2-bpy)$_2Cl_2$. In a typical procedure, poly-Ru(1,4-cyclooctadiene)$_2Cl_2$ (0.30 g, 0.97

DOI: 10.1021/ic501682k
Inorg. Chem. 2015, 54, 460−469

mmol) and 4,4′-R_2-bipyridine (where R = OCH_3, CH_3, or Br) (0.97 mmol) were dissolved in 1,2-dichlorobenzene (∼35 mL). The solution was thoroughly degassed with argon, and the mixture was heated to 180 °C under an atmosphere of argon for 2 h. The solution was cooled, ether (∼100 mL) was added, and the precipitate was isolated by suction filtration, washed with excess ether, and collected. These complexes were used without further purification. Yields ranged from 87 to 92%.

General Procedure for [Ru(4,4′-R_2-bpy)$_2$(PO_3H_2-bpy)]-(Cl)$_2$. In a typical procedure, Ru(4,4′-R_2-bpy)$_2$$Cl_2$ (0.12 mmol) and [2,2′-bipyridine]-4,4′-diyldiphosphonic acid (0.04 g, 0.12 mmol) were dissolved in 1:1 EtOH/H_2O (∼35 mL). The solution was then heated to 160 °C for 20 min in a microwave oven. The solution was cooled, filtered, and dried by a rotary evaporator. The crude product was purified by size exclusion chromatography (Sephadex LH-20) with 1:1 H_2O/MeOH as the eluent. Similar fractions (based on UV−vis absorption spectra) were combined, and the solvent was removed by rotary evaporation. The dark-red solids were triturated with ether and collected.

[Ru(4,4′-Dimethoxy-2,2′-bipyridine)$_2$([2,2′-bipyridine]-4,4′-diyldiphosphonic acid)]Cl_2 ***(RuPOMe)***. Isolated as a red powder (0.104 g, 90%). ^{1}H NMR (600 MHz, D_2O): δ (ppm) 8.67 (d, 2H), 8.11 (dd, 4H), 7.73 (m, 2H), 7.52 (m, 2H), 7.47 (d, 2H), 7.37 (d, 2H), 6.94 (dd, 2H), 6.89 (dd, 2H), 3.90 (s, 6H), 3.87 (s, 6H). HR-ESI-MS (MeOH; 20% H_2O with 1% HCOOH): m/z = 425.0457^{2+} = 850.09, [M − 2Cl$^-$]$^{2+}$ = 850.09, m/z = 849.0903^{2+} = 1698.1806, [M − 2Cl$^-$ − H$^+$]$_2^{2+}$ = 1698.16. Anal. found (calcd.) for $C_{35}H_{40}Cl_2N_6O_{12}P_2Ru$: C 43.53 (43.31), H 4.31 (4.15), N 8.84 (8.66).

[Ru(4,4′-Dimethyl-2,2′-bipyridine)$_2$([2,2′-bipyridine]-4,4′-diyldiphosphonic acid)]Cl_2 ***(RuPMe)***. Isolated as a red powder (0.099 g, 92%). ^{1}H NMR (600 MHz, D_2O): δ (ppm) 8.69 (d, 2H), 8.33 (d, 4H), 7.72 (m, 2H), 7.50 (m, 2H), 7.46 (m, 4H), 7.17 (m, 4H), 2.44 (s, 6H), 2.43 (s, 6H). HR-ESI-MS (80:20 NCMe/H_2O, 1% HCOOH): m/z = 384.0499^{2+} = 768.0996, [M − 2Cl$^-$]$^{2+}$ = 786.1059, m/z = 785.1042^{2+} = 1570.2084, [M − 2Cl$^-$ − H$^+$]$_2^{2+}$ = 1570.196. Anal. found (calcd.) for $C_{35}H_{38}Cl_2N_6O_7P_2Ru$: C 47.49 (47.31), H 4.50 (4.31), N 9.58 (9.46).

[Ru(2,2′-Bipyridine)$_2$([2,2′-bipyridine]-4,4′-diyldiphosphonic acid)]Cl_2 ***(RuP)***. Isolated as a red powder (0.086 g, 90%). The characterization matches that of a previously reported sample.[27]

[Ru(4,4′-Dibromo-2,2′-bipyridine)$_2$([2,2′-bipyridine]-4,4′-diyldiphosphonic acid)]Cl_2 ***(RuPBr)***. Isolated as a red powder (0.120 g, 87%). ^{1}H NMR (600 MHz, D_2O): δ (ppm) 8.94 (d, 4H), 8.73 (d, 2H), 7.71 (m, 2H), 7.62 (m, 8H), 7.52 (d, 2H). HR-ESI-MS (MeOH; 20% H_2O with 1% HCOOH): m/z = 522.8398^{2+} = 1045.6796, [M − 2Cl$^-$]$^{2+}$ = 1045.68. Anal. found (calcd.) for $C_{30}H_{28}Br_4Cl_2N_6O_9P_2Ru$: C 30.91 (30.79), H 2.52 (2.41), N 7.08 (7.18).

RESULTS AND DISCUSSION

Synthesis. 4,4′-Dibromo-bipyridine was synthesized by modifying a reported procedure starting from commercially available 4,4′-dimethoxy-bipyridine.[44] In previous studies, dimethylformamide (DMF) was used as the solvent for the reaction between PBr_3 and 4,4′-dimethoxy-bipyridine. Herein, 4,4′-dimethoxy-bipyridine was dissolved directly in PBr_3, heated to 180 °C, and the reaction was completed after 3 h and followed by TLC (Scheme 1). Following neutralization and extraction, purification was completed by passage through a silica plug, giving a 47% yield (Experimental Section). The 4,4′-(PO_3H_2)$_2$-bpy ligand was synthesized by a simple bromotrimethylsilane hydrolysis of the esterified ligand (4,4′-(PO_3Et_2)$_2$-bpy), which has been previously reported (Experimental Section).[27,45]

Scheme 1. Synthesis of 4,4′-Br-2,2′-Bipyridine

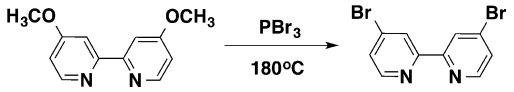

All of the complexes reported herein have the same general structure: [Ru(4,4′-R_2-bpy)$_2$(4,4′(PO_3H_2)$_2$-bpy)]$^{2+}$, where R = OCH_3, CH_3, H, or Br. The complexes were synthesized in good yields (87−92%) by a systematic procedure to vary the bidentate ligand, 4,4′-R_2-bpy. For the precursors, Ru(4,4′-R_2-bpy)$_2$$Cl_2$, 2 equiv of the 4,4′-$R_2$-bpy ligand was reacted with poly-Ru(1,4-cyclooctadiene)Cl_2[28] in *o*-dichlorobenzene at 180 °C for 2 h under an argon atmosphere (Experimental Section).[27] Poly-Ru(1,4-cyclooctadiene)Cl_2 was used as the precursor in the study because it inhibits the formation of [Ru(4,4′-R_2-bpy)$_3$]$^{2+}$ salts in the nonpolar *o*-dichlorobenzene.[27] Upon the addition of ether, the products, *cis*-Ru(4,4′-R_2-bpy)$_2$$Cl_2$, precipitate from the solution and were used without further purification (Scheme 2). Limited solubility makes the characterization of *cis*-Ru(4,4′-R_2-bpy)$_2$$Cl_2$ complexes difficult.

The chromophores were isolated as their chloride salts by the reaction of Ru(4,4′-R_2-bpy)$_2$$Cl_2$ with 1 equiv of 4,4′-(PO_3H_2)$_2$-bpy in 1:1 EtOH/H_2O in a microwave oven reactor at 160 °C for 20 min (Scheme 2). These reactions can be followed via UV−vis spectroscopy by monitoring the disappearance of Ru(4,4′-R_2-bpy)$_2$$Cl_2$[46] absorption features and the growth of [Ru(4,4′-R_2-bpy)$_2$(4,4′-(PO_3H_2)$_2$-bpy)]$^{2+}$ absorption features (Figure 5 and Table 2). The crude mixtures were each purified by size exclusion chromatography (Sephadex LH-20) to yield pure complexes.

The aromatic region of the ^{1}H NMR spectrum of each complex in D_2O is shown in Figure 2. The complexes have C_2 symmetry with a single 2-fold axis bisecting the 4,4′-(PO_3H_2)$_2$-bpy ligand. The C_2 symmetry is apparent in the ^{1}H NMR spectrum of each complex. There are three distinct resonances for the 4,4′-(PO_3H_2)$_2$-bpy ligands in each complex, appearing at ∼8.70, 7.75, and 7.50 ppm. The chemical shifts of these ligands remain relatively unaffected by the variation of the 4,4′-R_2-bpy ligand in the series (Figure 2). As expected, the proton resonances of the 4,4′-R_2-bpy ligands vary significantly through the series, with the more electron-poor 4,4′-(Br)$_2$-bpy ligand having resonances shifted downfield relative to those of the electron-rich 4,4′-(OCH_3)$_2$-bpy and 4,4′-(CH_3)$_2$-bpy ligands. In addition, as a result of the C_2 symmetry, the 4,4′-R_2-bpy ligands show six unique resonances for the six protons on each ligand.

Surface Binding. Adsorption isotherms were analyzed by the Langmuir isotherm model by immersing FTO|TiO_2 slides (7 μm) in solutions of complex in methanol (10, 20, 50, 100, 150, and 200 μM, Figure S2).[32] The adsorption constant (K_{ad}) and maximum surface coverage (Γ_{max}) for each complex are listed in Table 1. The absorption constants for all the complexes are similar: RuPOMe (1.8 × 10^5 M^{-1}), **RuPMe** (6.7 × 10^5 M^{-1}), **RuPBr** (1.5 × 10^5 M^{-1}), and **RuP** (0.39 × 10^5 M^{-1}, 1.3 × 10^5 M^{-1}).[47,48] Variation from the reported values for **RuP** and the other films studied herein is likely due to inconsistencies of the TiO_2 films used in this and previous

DOI: 10.1021/ic501682k
Inorg. Chem. 2015, 54, 460−469

Scheme 2. Syntheses of $Ru(4,4'\text{-}R_2\text{-}bpy)_2Cl_2$ and $[Ru(4,4'\text{-}R_2\text{-}bpy)_2(PO_3H_2)_2\text{-}bpy)]^{2+}$

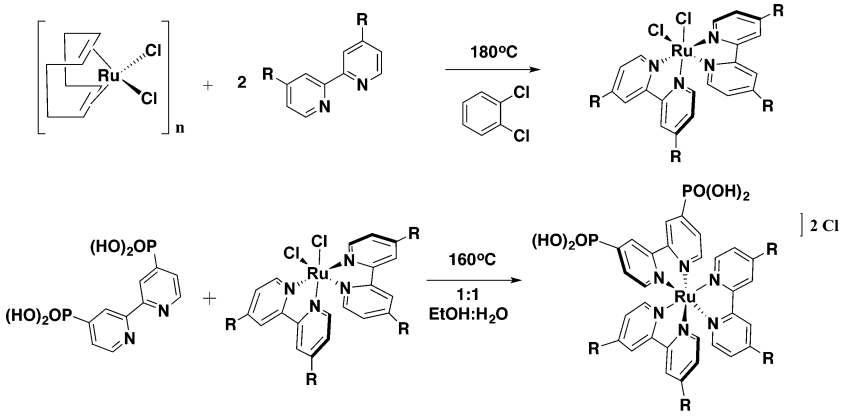

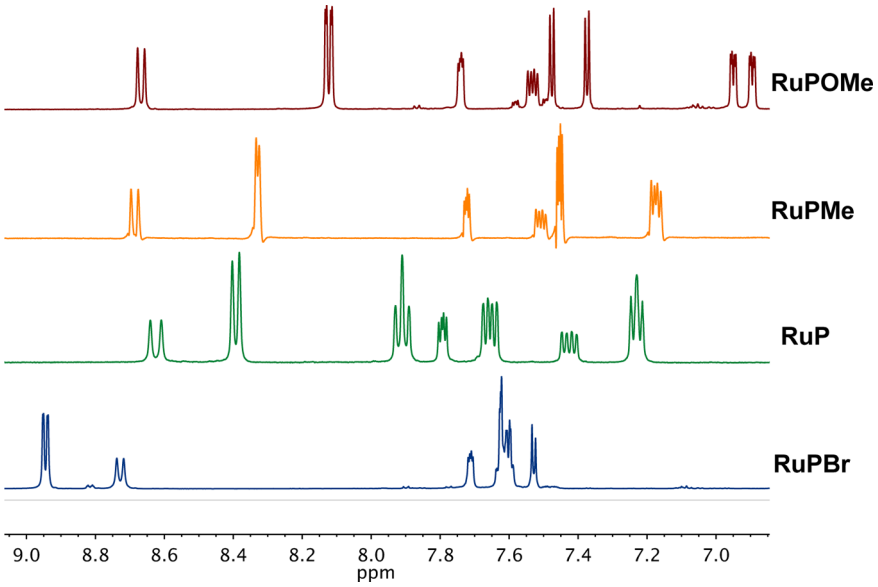

Figure 2. ^1H NMR in D_2O of **RuPBr** (blue), **RuP** (green), **RuPMe** (orange), and **RuPOMe** (red).

Table 1. Equilibrium Surface-Binding Parameters for RuPOMe, RuPMe, RuP, and RuPBr

complex	Γ_{max} (mol cm^{-2})[a]	K_{ad} ($M^{-1} \times 10^5$)
RuPOMe	6.7×10^{-8}	1.8
RuPMe	6.7×10^{-8}	6.7
RuP[b]	8.5×10^{-8}	1.3, 0.39
RuPBr	6.6×10^{-8}	1.5

[a]Maximum surface coverages are reported on the basis of a per micrometer thickness for 7 μm films. [b]Previously reported.[47,48]

studies.[19] The maximum surface coverages (Γ_{max}) range from 6.6×10^{-8} (**RuPBr**) to 8.5×10^{-8} mol cm^{-2} (**RuP**), suggesting similar packing of the complexes on the TiO_2 network.

Electrochemistry. The electrochemical properties of each complex in solution (80:20 CH_3CN/H_2O with 0.1 M $TBAPF_6$ supporting electrolyte, TBA = tetrabutylammonium) and immobilized on TiO_2 in aqueous $HClO_4$ (0.1 M) were investigated by cyclic and square-wave voltammetry. The CH_3CN/H_2O mixture (80:20) was used to investigate the ligand-based reduction potentials ($Ru^{2+/+}$) under conditions similar to those achieved using aqueous media without having a significant background H_2O reduction at the electrode.

All four complexes exhibit reversible $Ru^{3+/2+}$ redox couples, $E^{o\prime}$ versus NHE, both in solution and on mesoporous TiO_2 (eq 2, Table 2). The $Ru^{3+/2+}$ redox potentials, as measured by square-wave voltammograms (Table 2), are represented as $E^{o\prime}$ values measured versus either a Ag/AgCl (0.198 V vs NHE) or a $Ag/AgNO_3$ (0.40 V vs NHE) reference electrode and are cited "vs NHE". They follow the expected trend of increasing $E^{o\prime}$, following the sequence **RuPOMe** < **RuPMe** < **RuP** < **RuPBr**, with values ranging from 1.08 to 1.45 V (vs NHE) when immobilized on TiO_2 (Figure 3). The electronic nature of R in the $4,4'\text{-}R_2$-bpy ligand influences the π^* acceptor energy levels. In the complexes, the more electron-donating groups (R = OCH_3 or CH_3) destabilize the bpy-π^* orbitals, decreasing the extent of $d\pi-\pi^*$ back-bonding from Ru^{II} to the $4,4'\text{-}R_2$-bpy ligand. Decreased back-bonding destabilizes the $d\pi^6$ core, resulting in lowered $Ru^{3+/2+}$ redox potentials (Table 2). In contrast, the electron-withdrawing 4,4′-Br-bpy ligand stabilizes the π^*(bpy) orbitals, increasing $d\pi-\pi^*$ back-bonding, stabilizing the $d\pi^6$ configuration, and increasing $E^{o\prime}(Ru^{3+/2+})$.[17,49−51]

$$[Ru^{III}(N{-}N)_2(4,4'\text{-}(PO_3H_2)_2\text{-}bpy)]^{3+} \xrightarrow{+e^-} [Ru^{II}(N{-}N)_2(4,4'\text{-}(PO_3H_2)_2\text{-}bpy)]^{2+} \quad (2)$$

DOI: 10.1021/ic501682k
Inorg. Chem. 2015, 54, 460−469

Table 2. Summary of Photophysical, Electrochemical, and Surface-Binding Properties for RuPOMe, RuPMe, RuP, and RuPBr

complex	absorbance λ (ε)[a]	emission λ_{max}[b]	ΔG_{ES} (eV)[c]	$E^{o\prime}$ ($Ru^{3+/2+}$)[d]	$E^{o\prime}$ ($Ru^{3+/2+}$)[e]	$E^{o\prime}$ ($Ru^{2+/+}$)[e]	$E^{o\prime}$ ($Ru^{3+/2+*}$)[g]	$E^{o\prime}$ ($Ru^{2+*/+}$)[h]
RuPOMe	477 (11 800)	708	1.97	1.08	1.05	−1.33	−0.89	0.64
RuPMe	461 (12 800)	685	2.01	1.19	1.16	−1.33	−0.82	0.68
RuP	458 (12 00)	667	2.09	1.28	1.27	−1.29	−0.80	0.80
RuPBr	465 (13 400)	644	2.14	1.45	1.40	−1.09[f]	−0.69	1.05

[a]Absorbance λ represented in nanometers. Dominant metal-to-ligand charge transfer (MLCT), which is an absorption feature in H_2O, represented in mol L^{-1} cm^{-1}. [b]Emission λ_{max} represented in nanometers. Sample loaded onto ZrO_2 in argon-deaerated aqueous $HClO_4$ (0.1 M) at 23 °C. [c]Values for ΔG_{ES} are from a Franck−Condon analysis of emission spectra on ZrO_2 in aqueous $HClO_4$ (0.1 M); see text. [d]Values reported versus NHE from square-wave voltammograms in aqueous 0.1 M $HClO_4$. Measurements were carried out using an FTO|TiO_2 derivatized with a Ru-complex working electrode, a Pt-wire counter, and a Ag/AgCl reference electrode (0.198 V vs NHE). [e]Values reported versus NHE from square-wave voltammograms; samples were dissolved in a 80:20 CH_3CN/H_2O mixture deaerated with argon. Measurements were carried out using a glassy-carbon working electrode, a Pt-wire counter, and a $Ag/AgNO_3$ reference electrode (0.40 V vs NHE). [f]Irreversible redox couple. [g]$E^{o\prime}(Ru^{3+/2+*}) = E^{o\prime}(Ru^{3+/2+}) - \Delta G_{ES}$. [h]$E^{o\prime}(Ru^{2+*/+}) = E^{o\prime}(Ru^{2+/+}) + \Delta G_{ES}$.

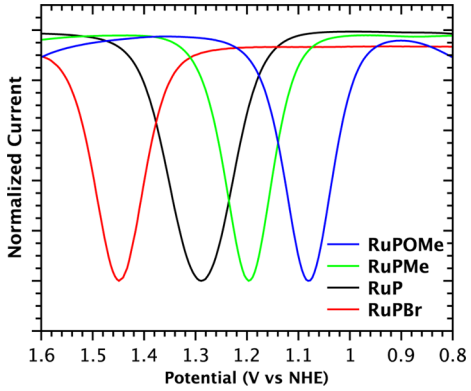

Figure 3. Square-wave voltammograms of **RuPOMe** (blue), **RuPMe** (green), **RuP** (black), and **RuPBr** (red), using derivatized FTO|TiO_2 as the working electrode, a Pt counter, and a Ag/AgCl reference electrode (0.198 V vs NHE) in aqueous $HClO_4$ (0.1 M).

The first ligand-based reduction potential ($E^{o\prime}(Ru^{2+/+})$) for each complex in solution (in 80:20 CH_3CN/H_2O, 0.1 M $TBAPF_6$ supporting electrolyte, Pt-wire counter, and Ag/$AgNO_3$ reference electrode) is listed in Table 2. The first reduction of the complexes follows a trend similar to that of the $E^{o\prime}(Ru^{3+/2+})$ couples with the most electron-withdrawing ligand (4,4′-Br_2-bpy in **RuPBr**) resulting in the most positive reduction potential. The first reduction of **RuPBr** (−1.09 V vs NHE) is significantly more positive than those of **RuP** (−1.29 V vs NHE), **RuPMe** (−1.33 V vs NHE), and **RuPOMe** (−1.33 V vs NHE). The positive shift from −1.33 V (**RuPOMe** and **RuPMe**) to −1.09 V (**RuPBr**) is due to the lowering of the energy of the π^*-acceptor orbitals of 4,4′-Br_2-bpy relative to those of 4,4′-$(OCH_3)_2$-bpy or 4,4′-$(CH_3)_2$-bpy; this is attributable to the electron-withdrawing Br atoms in the bipyridine framework. **RuPOMe**, **RuPMe**, and **RuP** have similar first-reduction potentials, which is consistent with a largely 4,4′-$(PO_3H_2)_2$-bpy-based assignment (eq 3). In contrast, the first reduction of **RuPBr** is significantly more positive, pointing to a reduction at 4,4′-$(Br)_2$-bpy (eq 4).

$$[Ru^{II}(4,4'\text{-}R_2\text{-bpy})_2(4,4'\text{-}(PO_3H_2)_2\text{-bpy})]^{2+} \xrightarrow{+e^-} [Ru^{II}(4,4'\text{-}R_2\text{-bpy})_2(4,4'\text{-}(PO_3H_2)_2\text{-bpy}^{\cdot-})]^{+} \quad (3)$$

$$[Ru^{II}(4,4'\text{-}Br_2\text{-bpy})_2(4,4'\text{-}(PO_3H_2)_2\text{-bpy})]^{2+} \xrightarrow{+e^-} [Ru^{II}(4,4'\text{-}Br_2\text{-bpy}^{\cdot-})(4,4'\text{-}Br_2\text{-bpy})(4,4'\text{-}PO_3H_2)_2\text{-bpy})]^{+} \quad (4)$$

Each complex shows multiple reduction waves within the potential window of the experiments with scans extended to −1.8 V versus NHE. As an example, three ligand-based reduction waves appear for **RuPMe** between −0.8 V and −1.8 V (vs NHE), Figure 4, arising from reduction at 4,4′-$(PO_3H_2)_2$-bpy followed by reduction at both of the 4,4′-$(CH_3)_2$-bpy ligands.

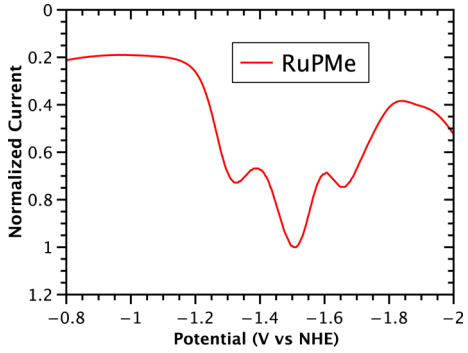

Figure 4. Square-wave voltammogram for **RuPMe**, using 1.0 mM of the complex dissolved in an 80:20 mixture of CH_3CN/H_2O, a 0.1 M $TBAPF_6$ supporting electrolyte, a Pt-wire counter, and a $Ag/AgNO_3$ reference (0.40 V vs NHE).

UV−Vis Absorption Spectra. The absorption spectra of all of the complexes in aqueous solution feature intense $\pi \rightarrow \pi^*$ absorptions below 350 nm ($\varepsilon \approx 4.3 \times 10^4$−$5.7 \times 10^4$ M^{-1} cm^{-1}) and lower-energy metal-to-ligand charge-transfer (MLCT) absorptions from 400 to 500 nm (Figure 5 and Table 2, single spectra are available in the Supporting Information). Although there are slight variations in MLCT $\lambda_{max,abs}$ values in the series, there is no obvious correlation between the electron-donating or -withdrawing nature of the 4,4′-R_2-bpy ligands and these values. The lack of correlation shows that although the dπ orbitals are stabilized by the electron-withdrawing 4,4′-R_2-bpy ligands resulting in an

DOI: 10.1021/ic501682k
Inorg. Chem. 2015, 54, 460−469

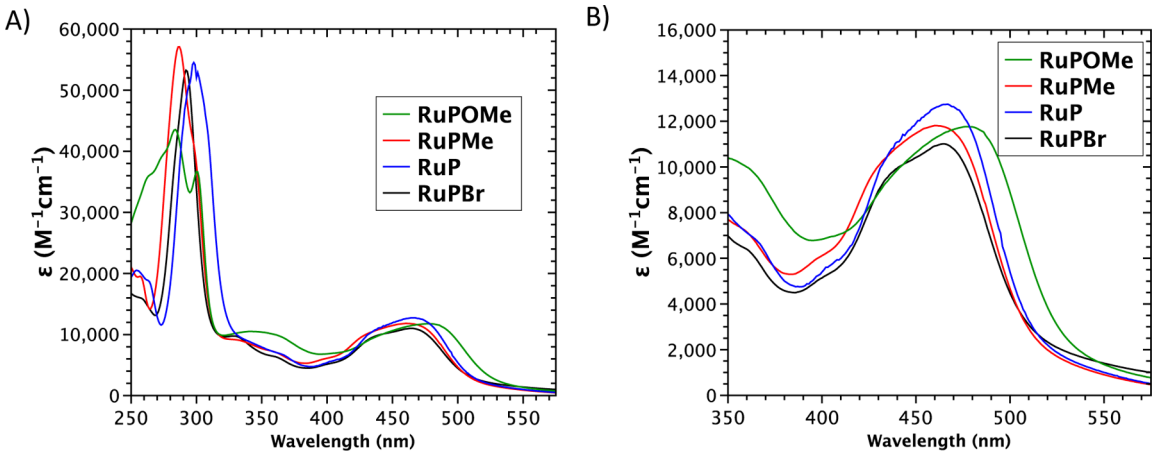

Figure 5. UV−visible absorption spectra of **RuPOMe**, **RuPMe**, **RuP**, and **RuPBr** dissolved in unbuffered H_2O, pH ≈ 6.5, at 23 °C.

Table 3. TD-DFT-Calculated MLCT Absorption Energies and Oscillator Strengths in Water

chromophore	excitation (nm)	oscillator strength	orbital contribution
RuPOMe	460	0.18	Ru dπ → π^* $(PO_3H_2)_2$-bpy
	409	0.1	Ru dπ → π^* OMe-bpy
RuPMe	455	0.126	Ru dπ → π^* $(PO_3H_2)_2$-bpy
	411	0.155	Ru dπ → π^* Me-bpy
RuP	443	0.179	Ru dπ → π^* $(PO_3H_2)_2$-bpy
	411	0.153	Ru dπ → π^* bpy
RuPBr	431	0.18	Ru dπ → π^* Br-bpy + π^* $(PO_3H_2)_2$-bpy
	429	0.2	Ru dπ → π^* $(PO_3H_2)_2$-bpy + π^* Br-bpy

increase in $E^{o\prime}(Ru^{3+/2+})$ there is a compensating stabilization in the energies of the π^*-acceptor orbitals.

TD DFT calculations were performed to justify and to quantify the spectral assignments associated with the electronic transitions (Figure S6). Complex geometries were optimized using DFT (B3LYP/LanL2DZ functional/basis set), and optimized geometries were used in the TD DFT (PBE0/LanL2DZ functional/basis set) calculations with a continuum model to account for solvation by H_2O. The computed spectra are blueshifted relative to the experimental spectra, which is likely caused by the inherent TD DFT overestimation of MLCT energies in Ru polypyridyl complexes as well as solvent effects that are not adequately described by the PCM used here.[16,52] Nevertheless, the experimental and computed spectra correlate well with the strong $\pi \rightarrow \pi^*$ absorptions predicted below 300 nm and MLCT absorptions at longer wavelengths (Table 3 and Figure S6). The calculations verify the origins of the visible absorptions as excitations arising from d$\pi \rightarrow \pi^*$ transitions to either the 4,4′-R_2-bpy ligand (eq 5) or the 4,4′-$(PO_3H_2)_2$-bpy ligand (eq 6). Furthermore, TD DFT predicts that MLCT transitions to the ancillary 4,4′-R_2-bpy ligand in **RuP**, **RuPMe**, and **RuPOMe** are higher in energy than those to the 4,4′-$(PO_3H_2)_2$-bpy ligand (Table 3).

$$[Ru^{II}(4,4'\text{-}R_2\text{-bpy})_2(4,4'\text{-}(PO_3H_2)_2\text{-bpy})]^{2+} \xrightarrow{h\nu} [Ru^{II}(4,4'\text{-}R_2\text{-bpy}^{\cdot-})(4,4'\text{-}R_2\text{-bpy})(4,4'\text{-}(PO_3H_2)_2\text{-bpy})]^{2+*} \quad (5)$$

$$[Ru^{II}(4,4'\text{-}R_2\text{-bpy})_2(4,4'\text{-}(PO_3H_2)_2\text{-bpy})]^{2+} \xrightarrow{h\nu} [Ru^{II}(4,4'\text{-}R_2\text{-bpy})_2(4,4'\text{-}(PO_3H_2)_2\text{-bpy}^{\cdot-})]^{2+*} \quad (6)$$

Figure 6 compares the calculated and the experimental electronic absorption spectra for **RuPMe** in H_2O; the calculated

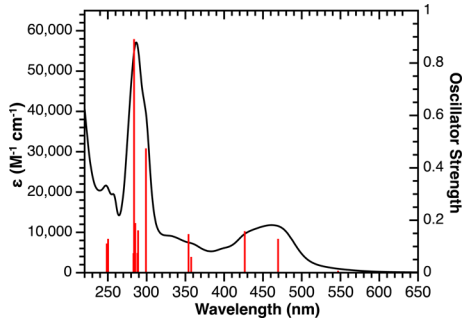

Figure 6. UV−visible spectrum of **RuPMe** at 23 °C in H_2O (black line) and calculated TD DFT transitions (vertical red bars, the heights of these illustrate the oscillator strengths red-shifted by 0.15 eV).

transition energies are shown as vertical bars whose heights reflect their relative oscillator strengths. The calculations show the split in the MLCT manifold between the MLCT transitions to π^*(4,4′-$(CH_3)_2$-bpy) and to π^*(4,4′-$(PO_3H_2)_2$-bpy) with the higher-energy MLCT Ru d$\pi \rightarrow \pi^*$ (4,4′-$(CH_3)_2$-bpy) (eq 5) and the lower-energy MLCT Ru d$\pi \rightarrow \pi^*$(4,4′-$(PO_3H_2)_2$-bpy) (eq 6). Figure S7 shows the orbital contribution for both transitions.

Steady-State Emission Spectra. All four complexes exhibit broad emission spectra at room temperature when surface-bound to ZrO_2 in deaerated aqueous $HClO_4$ (0.1 M). The emission spectrum for each complex is shown in Figure 7, and the emission energies are listed in Table 2. The emission energies decrease from **RuPBr** (λ_{max} = 644 nm, 1.55 × 10^4 cm^{-1}) to **RuPOMe** (λ_{max} = 708 nm, 1.41 × 10^4 cm^{-1}). Emission from these complexes occurs from the lowest-lying ^{3}MLCT excited states, following intersystem crossing from the initial ^{1}MLCT excited states that dominate absorption.[16,17,53,54]

DOI: 10.1021/ic501682k
Inorg. Chem. 2015, 54, 460−469

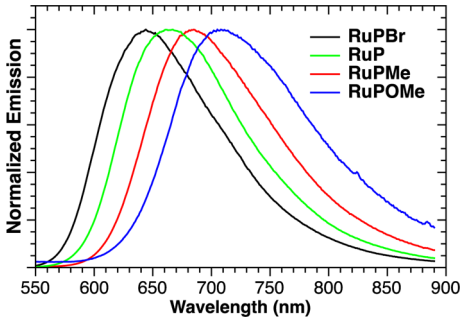

Figure 7. Normalized emission spectra of **RuPBr** (black), **RuP** (green), **RuPMe** (red), and **RuPOMe** (blue); samples were loaded onto ZrO_2 ($\Gamma \approx 8 \times 10^{-8}$ mol cm^{-2}) in argon-deaerated aqueous $HClO_4$ (0.1 M) at 23 °C following excitation at 450 nm.

Trends in the emission energies ($\lambda_{max,em}$, $\overline{\nu}_{em}$) follow those of $E^{o\prime}(Ru^{3+/2+})$, with more positive values resulting in higher emission energies. This is illustrated in Figure 8 by the linear

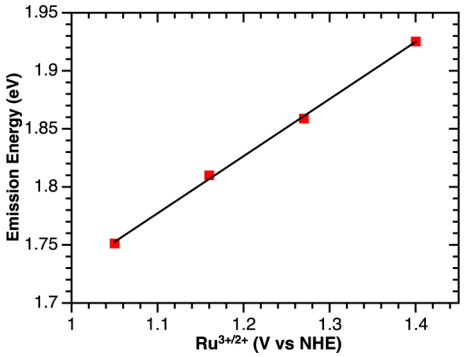

Figure 8. Dependence of emission energy ($\lambda_{max,em}$, $\overline{\nu}_{em}$) on $E^{o\prime}(Ru^{3+/2+})$ in aqueous $HClO_4$ (0.1 M) at 25 °C; samples were bound to a metal oxide surface (TiO_2 for $E^{o\prime}(Ru^{3+/2+})$ and ZrO_2 for $\overline{\nu}_{em}$).

dependence of the emission energy on $E^{o\prime}(Ru^{3+/2+})$. This suggests that variations in excited-state energies with ligand changes are mainly a consequence of variations in the energy of the metal-based dπ orbitals.[16,55] There is no correlation between emission energies and the ligand-based $E^{o\prime}(Ru^{2+/+})$ values (Figure S8).

EMISSION-SPECTRA FITTING: CORRELATION OF EXCITED-STATE PROPERTIES

Emission spectra for all complexes bound to ZrO_2 in aqueous $HClO_4$ (0.1 M) at 25 °C were analyzed by use of a single-mode Franck–Condon analysis.[16,19,56−60] In this analysis, the contributions from medium-frequency (ν) modes (bpy) are treated as a single averaged mode with low-frequency modes and the solvent included in the band widths. Emission spectra were fit to a series of vibronic lines centered on the 0–0 component at energy E_0 and separated by a vibrational quantum spacing of $\hbar\omega_M$. Only the transitions from the $\nu' = 0$ level in the excited state to level ν in the ground state were included in the summation.

In the spectral fits, relative intensities of the vibronic lines are determined by the electron-vibrational coupling constant, S_M, which is related to the equilibrium displacement change, ΔQ_{eq}, by $^1/_2(\Delta Q_{eq})^2$. As noted above, additional vibrational contributions from low-frequency modes and the solvent are treated classically and included in the bandwidth at half height, $\Delta\overline{\nu}_{1/2}$, with $\Delta\overline{\nu}_{1/2}$ defined in eq 7. In eq 7, $\lambda_{0,L}$ is the sum of the solvent reorganization energy, λ_0, and reorganization energy from low-frequency modes, λ_L; E_0 is the 0–0 energy gap, the energy of the excited state above the ground state with both states in the $\nu = 0$ vibrational levels; k_B is the Boltzmann constant; and T is the temperature (298 K).

$$\Delta G_{ES} = E_0 + \lambda_{0,L} = E_0 + \frac{(\Delta\nu_{1/2})^2}{16k_BT \ln 2} \quad (7)$$

Results of the spectra-fitting analysis are summarized in Table 4. The free-energy content of the excited states (ΔG_{ES})

Table 4. Emission-Spectra Fitting Parameters Derived from MLCT Photoluminescence of RuPOMe, RuPMe, RuP, and RuPBr Loaded onto ZrO_2 in Deaerated Aqueous $HClO_4$ (0.1 M) at 25 °C

complex	E_0 (cm^{-1})	$\Delta\overline{\nu}_{1/2}$ (cm^{-1})	$\hbar\omega_M$ (cm^{-1})	S_M	ΔG_{ES} (cm^{-1})
RuPOMe	14 300	1920	1350	0.89	15 900
RuPMe	14 700	1850	1350	0.86	16 200
RuP	15 200	1930	1350	0.79	16 800
RuPBr	15 700	1870	1350	0.90	17 300

were calculated by using eq 7. As shown in Tables 2 and 4, trends in ΔG_{ES} mirror those of the emission energies across the series. Both the free-energy content of the excited state (ΔG_{ES}) and the 0–0 energy gap (E_0) increase as $E^{o\prime}(Ru^{3+/2+})$ increases (Figure 9). This trend is expected because the emission energy is dependent on the energy of the dπ levels rather than on the π^* levels (see above and Figure 8).

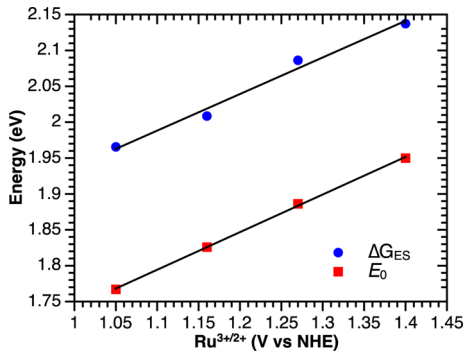

Figure 9. Dependence of the free-energy content of the excited state (ΔG_{ES}, blue circles) and the 0–0 energy gap (E_0) on the ground-state oxidation potential ($E^{o\prime}(Ru^{3+/2+})$) for **RuPOMe**, **RuPMe**, **RuP**, and **RuPBr**.

EXCITED-STATE REDOX POTENTIALS

A motivation for synthesizing and characterizing this series of complexes was to explore the role of ancillary ligand variation on the light-absorption and redox properties of a series of surface-bound complexes that could be used for possible photoelectrochemical applications. As noted in the Introduction, key properties are broad light absorption in the visible spectrum, excited-state electron injection into the conduction bands of high-band-gap semiconductors, and sufficient potential to drive water-oxidation catalysis as Ru^{3+}. In the current series of complexes, the dominating MLCT absorptions

DOI: 10.1021/ic501682k
Inorg. Chem. 2015, 54, 460–469

in the visible spectrum remain relatively constant across the series (Figure 5), even with significant variations in $E^{o\prime}(Ru^{3+/2+})$ and $E^{o\prime}(Ru^{2+/+})$ (Figure 1 and Table 2).

To quantify the impact of ligand variation on excited-state redox potentials, $E^{o\prime}$ values for the excited state acting as an oxidant, $Ru^{2+*/+}$ (eq 8), and reductant, $Ru^{3+/2+*}$ (eq 9), were calculated from the ground-state potentials in Table 1 and the free energies of the excited state above the ground state, ΔG_{ES}, determined by emission-spectra fitting in Table 2.[16,18,23,55]

$$E^{o\prime}(Ru^{2+*/+}) = E^{o\prime}(Ru^{2+/+}) + \Delta G_{ES} \quad (8)$$

$$E^{o\prime}(Ru^{3+/2+*}) = E^{o\prime}(Ru^{3+/2+}) - \Delta G_{ES} \quad (9)$$

Similar to the correlations previously reported for complexes of the type $[M(bpy)_2(L)]^{2+}$ (where M = Ru^{II} or Os^{II} and L is a bidentate, neutral four-electron-donor ligand), metal-based potentials for both ground-state $Ru^{3+/2+}$ ($d\pi^5/d\pi^6$) and excited-state $Ru^{2+*/+}$ ($d\pi^5\pi^{*1}/d\pi^6\pi^{*1}$) redox couples decrease linearly with emission energy.[61−63] In contrast, the ligand-centered ground-state $Ru^{2+/+}$ ($d\pi^6/d\pi^6\pi^1$) and excited-state $Ru^{3+/2+*}$ ($d\pi^5/d\pi^5\pi^{*1}$) couples decrease by only half the magnitude of $Ru^{2+*/+}$ and $Ru^{3+/2+}$ potentials (Figure 10). These observations reinforce the conclusion that variations in Ru-dπ levels (and not variations in π^*(bpy)) are the major factor influencing excited-state redox potentials.

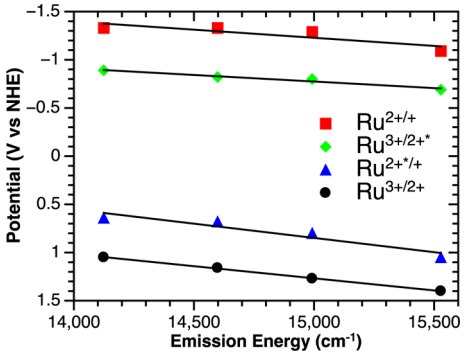

Figure 10. Variation of ground- and excited-state redox potentials with variation of the emission energy for each complex.

Figure 11 illustrates the variation of $E^{o\prime}(Ru^{3+/2+*})$ with variation of $E^{o\prime}(Ru^{3+/2+})$ across the series. An important feature in the data is the increase in oxidizing strength of Ru^{3+} across

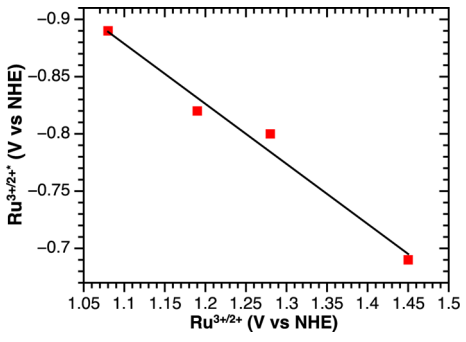

Figure 11. Variation of the excited-state reduction potential ($Ru^{3+/2+*}$) with variation of the ground-state oxidation potential ($Ru^{3+/2+}$).

the series with variations in $E^{o\prime}(Ru^{3+/2+})$ that are induced by varying the 4,4′-R_2-bpy ligand from 1.08 to 1.45 V (vs NHE). The enhanced oxidative-ground-state potential for Ru^{3+} comes at the price of a decrease in the excited-state oxidation potential, with $E^{o\prime}(Ru^{3+/2+*})$ increasing in the same series from −0.89 to −0.69 V (vs NHE).

As a particular example, $E^{o\prime}(Ru^{3+/2+})$ for **RuPBr** immobilized on TiO_2 in aqueous $HClO_4$ (0.1 M) is 1.45 V (vs NHE) with light-absorption properties comparable to those of **RuP** (Figure 5). An $E^{o\prime}$ of this magnitude provides the thermodynamic basis for driving water-oxidation catalysis. However, the exchange of bpy for 4,4′-Br_2-bpy increases $E^{o\prime}(Ru^{3+/2+*})$ from −0.80 to −0.69 V (vs NHE), lowering the thermodynamic driving force for electron injection and likely resulting in slower and less efficient electron injection.[5,24,64] Analysis of electron injection efficiencies and kinetics is currently under investigation for this series of complexes.

CONCLUSIONS

We describe here the study of a series of polypyridyl complexes in which ligand variations were used systematically to modify excited- and ground-state properties of the complexes. A target was the synthesis of a series of Ru(II) polypyridyl chromophores for potential applications in DSPEC devices. The approach taken was to prepare a family of chromophores with the common 4,4′-$(PO_3H_2)_2$-bpy ligand for surface-binding to oxides, with variations in the remaining ligands being used to modify the electronic structure and thus alter light-absorption and excited-state properties, including redox properties. Variations in the polypyridyl ligand have been shown to result in a related series of complexes in which the ground-state $E^{o\prime}(Ru^{3+/2+})$ values vary from 1.08 to 1.45 V (vs NHE) without significant loss in visible light absorption, as observed by UV−visible spectroscopy and analyzed by TD DFT calculations. The insensitivity of light absorption to ligand changes is due to the changes in ligand π^* acceptor levels being compensated for by changes in dπ levels, resulting in a nearly constant energy gap. This electronic-compensation effect results in enhanced ground-state oxidizing strength and a parallel decrease in excited-state reducing strength, with the latter decreasing the driving force for electron injection.

ASSOCIATED CONTENT

Supporting Information

UV−visible spectra, square-wave voltammograms, TD DFT results, surface-loading isotherms, orbitals contributing to the MLCT exitations for **RuPMe**, and plot of variation of $\overline{\nu}_{em}(\lambda_{max,em})$ for **RuP**, **RuPBr**, **RuPMe**, and **RuPOMe**. This material is available free of charge via the Internet at http://pubs.acs.org.

AUTHOR INFORMATION

Corresponding Author

*E-mail: tjmeyer@unc.edu.

Present Address

J.J.C.: Chemistry Department, Building 555, Brookhaven National Laboratory, P.O. Box 5000, Upton, New York 11973-5000, United States.

Notes

The authors declare no competing financial interest.

DOI: 10.1021/ic501682k
Inorg. Chem. 2015, 54, 460−469

■ ACKNOWLEDGMENTS

This work was primarily supported by the UNC Energy Frontier Research Center (EFRC) for Solar Fuels, an EFRC funded by the U.S. Department of Energy, Office of Science, and Office of Basic Energy Sciences (DOE BES) under award DE-SC0001011, supporting M.K.B., R.J.B., S.K., and J.J.C. We thank the Department of Energy Office of Science Graduate Fellowship Program (DOE SCGF) for a fellowship for D.L.A., made possible by the American Recovery and Reinvestment Act of 2009, administered by ROISE-ORAU under contract number DE-AC05-06OR23100.

■ REFERENCES

(1) Hagfeldt, A.; Boschloo, G.; Sun, L.; Kloo, L.; Pettersson, H. *Chem. Rev.* **2010**, *110*, 6595.
(2) Song, W.; Chen, Z.; Glasson, C. R.; Hanson, K.; Lou, H.; Norris, M. R.; Ashford, D. L.; Concepcion, J. J.; Brennaman, M. K.; Meyer, T. J. *ChemPhysChem* **2012**, *13*, 2882.
(3) Bard, A. J.; Fox, M. A. *Acc. Chem. Res.* **1995**, *28*, 141.
(4) Concepcion, J. J.; Jurss, J. W.; Brennaman, M. K.; Hoertz, P. G.; Patrocinio, A. O. T.; Murakami Iha, N. Y.; Templeton, J. L.; Meyer, T. J. *Acc. Chem. Res.* **2009**, *42*, 1954.
(5) Swierk, J. R.; Mallouk, T. E. *Chem. Soc. Rev.* **2013**, *42*, 2357.
(6) Youngblood, W. J.; Lee, S.-H. A.; Maeda, K.; Mallouk, T. E. *Acc. Chem. Res.* **2009**, *42*, 1966.
(7) Young, K. J.; Martini, L. A.; Milot, R. L.; Snoeberger, R. C.; Batista, V. S.; Schmuttenmaer, C. A.; Crabtree, R. H.; Brudvig, G. W. *Coord. Chem. Rev.* **2012**, *256*, 2503.
(8) Gust, D.; Moore, T. A.; Moore, A. L. *Acc. Chem. Res.* **2009**, *42*, 1890.
(9) Wasielewski, M. R. *Acc. Chem. Res.* **2009**, *42*, 1910.
(10) Alstrum-Acevedo, J. H.; Brennaman, M. K.; Meyer, T. J. *Inorg. Chem.* **2005**, *44*, 6802.
(11) Kay, A.; Graetzel, M. *J. Phys. Chem.* **1993**, *97*, 6272.
(12) Ashford, D. L.; Song, W.; Concepcion, J. J.; Glasson, C. R.; Brennaman, M. K.; Norris, M. R.; Fang, Z.; Templeton, J. L.; Meyer, T. J. *J. Am. Chem. Soc.* **2012**, *134*, 19189.
(13) Gratzel, M. *Acc. Chem. Res.* **2009**, *42*, 1788.
(14) Argazzi, R.; Bignozzi, C. A.; Heimer, T. A.; Castellano, F. N.; Meyer, G. J. *J. Phys. Chem. B* **1997**, *101*, 2591.
(15) Anderson, N. A.; Lian, T. *Coord. Chem. Rev.* **2004**, *248*, 1231.
(16) Ashford, D. L.; Glasson, C. R. K.; Norris, M. R.; Hanson, K.; Concepcion, J. J.; Keinan, S.; Brennaman, M. K.; Templeton, J. L.; Meyer, T. J. *Inorg. Chem.* **2014**, *53*, 5637.
(17) Yam, V. W.-W.; Lee, V. W.-M.; Ke, F.; Siu, K.-W. M. *Inorg. Chem.* **1997**, *36*, 2124.
(18) Thompson, D. W.; Ito, A.; Meyer, T. J. *Pure Appl. Chem.* **2013**, *85*, 1257.
(19) Hanson, K.; Brennaman, M. K.; Ito, A.; Luo, H.; Song, W.; Parker, K. A.; Ghosh, R.; Norris, M. R.; Glasson, C. R. K.; Concepcion, J. J.; Lopez, R.; Meyer, T. J. *J. Phys. Chem. C* **2012**, *116*, 14837.
(20) Hanson, K.; Brennaman, M. K.; Luo, H.; Glasson, C. R. K.; Concepcion, J. J.; Song, W.; Meyer, T. J. *ACS Appl. Mater. Interfaces* **2012**, *4*, 1462.
(21) Ashford, D. L.; Lapides, A. M.; Vannucci, A. K.; Hanson, K.; Torelli, D. A.; Harrison, D. P.; Templeton, J. L.; Meyer, T. J. *J. Am. Chem. Soc.* **2014**, *136*, 6578.
(22) Norris, M. R.; Concepcion, J. J.; Fang, Z.; Templeton, J. L.; Meyer, T. J. *Angew. Chem., Int. Ed.* **2013**, *52*, 13580.
(23) Ardo, S.; Meyer, G. J. *Chem. Soc. Rev.* **2009**, *38*, 115.
(24) Gratzel, M. *Nature* **2001**, *414*, 338.
(25) Gratzel, M. *J. Photochem. Photobiol., C* **2003**, *4*, 145.
(26) Asbury, J. B.; Hao, E.; Wang, Y.; Ghosh, H. N.; Lian, T. *J. Phys. Chem. B* **2001**, *105*, 4545.
(27) Norris, M. R.; Concepcion, J. J.; Glasson, C. R. K.; Fang, Z.; Lapides, A. M.; Ashford, D. L.; Templeton, J. L.; Meyer, T. J. *Inorg. Chem.* **2013**, *52*, 12492.
(28) Doi, T.; Nagamiya, H.; Kokubo, M.; Hirabayashi, K.; Takahashi, T. *Tetrahedron* **2002**, *58*, 2957.
(29) Lee, S.-H. A.; Abrams, N. M.; Hoertz, P. G.; Barber, G. D.; Halaoui, L. I.; Mallouk, T. E. *J. Phys. Chem. B* **2008**, *112*, 14415.
(30) Song, W.; Glasson, C. R. K.; Luo, H.; Hanson, K.; Brennaman, M. K.; Concepcion, J. J.; Meyer, T. J. *J. Phys. Chem. Lett.* **2011**, *2*, 1808.
(31) Gallagher, L. A.; Serron, S. A.; Wen, X.; Hornstein, B. J.; Dattelbaum, D. M.; Schoonover, J. R.; Meyer, T. J. *Inorg. Chem.* **2005**, *44*, 2089.
(32) Langmuir, I. *J. Am. Chem. Soc.* **1918**, *40*, 1361.
(33) Becke, A. D. *J. Chem. Phys.* **1993**, *98*, 5648.
(34) Lee, C.; Yang, W.; Parr, R. G. *Phys. Rev. B* **1988**, *37*, 785.
(35) Dunning, T. H., Jr.; Hay, P. J. In *Methods of Electronic Stucture Theory*; Schaefer, H. F., III, Ed.; Modern Theoretical Chemistry Series; Plenum Press: New York, 1976; Vol. 3, pp 1−27.
(36) Wadt, W. R.; Hay, P. J. *J. Chem. Phys.* **1985**, *82*, 284.
(37) Jacquemin, D.; Perpete, E. A.; Scuseria, G. E.; Ciofini, I.; Adamo, C. *J. Chem. Theory Comput.* **2008**, *4*, 123.
(38) Jacquemin, D.; Preat, J.; Perpete, E. A.; Adamo, C. *Int. J. Quantum Chem.* **2010**, *110*, 2121.
(39) Perdew, J. P.; Burke, K.; Ernzerhof, M. *Phys. Rev. Lett.* **1996**, *77*, 3865.
(40) Adamo, C.; Barone, V. *J. Chem. Phys.* **1999**, *110*, 6158.
(41) Bauernschmitt, R.; Ahlrichs, R. *Chem. Phys. Lett.* **1996**, *256*, 454.
(42) Frisch, M. J.;Trucks, G. W.; Schlegel, H. B.; Scuseria, G. E.; Robb, M. A.; Cheeseman, J. R.; Scalmani, G.; Barone, V.; Mennucci, B.; Petersson, G. A.; Nakatsuji, H.; Caricato, M.; Li, X.; Hratchian, H. P.; Izmaylov, A. F.; Bloino, J.; Zheng, G.; Sonnenberg, J. L.; Hada, M.; Ehara, M.; Toyota, K.; Fukuda, R.; Hasegawa, J.; Ishida, M.; Nakajima, T.; Honda, Y.; Kitao, O.; Nakai, H.; Vreven, T.; Montgomery, J. A., Jr.; Peralta, J. E.; Ogliaro, F.; Bearpark, M.; Heyd, J. J.; Brothers, E.; Kudin, K. N.; Staroverov, V. N.; Kobayashi, R.; Normand, J.; Raghavachari, K.; Rendell, A.; Burant, J. C.; Iyengar, S. S.; Tomasi, J.; Cossi, M.; Rega, N.; Millam, J. M.; Klene, M.; Knox, J. E.; Cross, J. B.; Bakken, V.; Adamo, C.; Jaramillo, J.; Gomperts, R.; Stratmann, R. E.; Yazyev, O.; Austin, A. J.; Cammi, R.; Pomelli, C.; Ochterski, J. W.; Martin, R. L.; Morokuma, K.; Zakrzewski, V. G.; Voth, G. A.; Salvador, P.; Dannenberg, J. J.; Dapprich, S.; Daniels, A. D.; Farkas, Ö.; Foresman, J. B.; Ortiz, J. V.; Cioslowski, J.; Fox, D. J. *Gaussian 09*, Revision C.01; Gaussian, Inc.: Wallingford, CT, 2009.
(43) Han, W.-S.; Han, J.-K.; Kim, H.-Y.; Choi, M. J.; Kang, Y.-S.; Pac, C.; Kang, S. O. *Inorg. Chem.* **2011**, *50*, 3271.
(44) Ma, J.; Wu, J.; Liu, W.; Wang, P.; Fan, Z. *Spectrochim. Acta, Part A* **2012**, *94*, 340.
(45) Hata, T.; Yamada, K.; Futatsugi, T.; Sekine, M. *Synthesis* **1979**, 189.
(46) Gu, J.; Chen, J.; Schmehl, R. H. *J. Am. Chem. Soc.* **2010**, *132*, 7338.
(47) Lapides, A. M.; Ashford, D. L.; Hanson, K.; Torelli, D. A.; Templeton, J. L.; Meyer, T. J. *J. Am. Chem. Soc.* **2013**, *135*, 15450.
(48) Gillaizeau-Gauthier, I.; Odobel, F.; Alebbi, M.; Argazzi, R.; Costa, E.; Bignozzi, C. A.; Qu, P.; Meyer, G. J. *Inorg. Chem.* **2001**, *40*, 6073.
(49) Rillema, D. P.; Mack, K. B. *Inorg. Chem.* **1982**, *21*, 3849.
(50) Ji, S.; Wu, W.; Wu, W.; Song, P.; Han, K.; Wang, Z.; Liu, S.; Guo, H.; Zhao, J. *J. Mater. Chem.* **2010**, *20*, 1953.
(51) Ackermann, M. N.; Interrante, L. V. *Inorg. Chem.* **1984**, *23*, 3904.
(52) Kapovsky, M.; Dares, C.; Dodsworth, E. S.; Begum, R. A.; Raco, V.; Lever, A. B. P. *Inorg. Chem.* **2012**, *52*, 169.
(53) Caspar, J. V.; Meyer, T. J. *Inorg. Chem.* **1983**, *22*, 2444.
(54) Van Houten, J.; Watts, R. J. *J. Am. Chem. Soc.* **1976**, *98*, 4853.
(55) Kober, E. M.; Marshall, J. L.; Dressick, W. J.; Sullivan, B. P.; Caspar, J. V.; Meyer, T. J. *Inorg. Chem.* **1985**, *24*, 2755.
(56) Caspar, J. V.; Meyer, T. J. *J. Am. Chem. Soc.* **1983**, *105*, 5583.
(57) Knight, T. E.; Goldstein, A. P.; Brennaman, M. K.; Cardolaccia, T.; Pandya, A.; DeSimone, J. M.; Meyer, T. J. *J. Phys. Chem. B* **2011**, *115*, 64.

DOI: 10.1021/ic501682k
Inorg. Chem. 2015, 54, 460−469

(58) Nozaki, K.; Takamori, K.; Nakatsugawa, Y.; Ohno, T. *Inorg. Chem.* **2006**, *45*, 6161.
(59) Kim, H. B.; Kitamura, N.; Tazuke, S. *J. Phys. Chem.* **1990**, *94*, 7401.
(60) Ito, A.; Meyer, T. J. *Phys. Chem. Chem. Phys.* **2012**, *14*, 13731.
(61) Li, J.; Djurovich, P. I.; Alleyne, B. D.; Yousufuddin, M.; Ho, N. N.; Thomas, J. C.; Peters, J. C.; Bau, R.; Thompson, M. E. *Inorg. Chem.* **2005**, *44*, 1713.
(62) Vogler, L. M.; Jones, S. W.; Jensen, G. E.; Brewer, R. G.; Brewer, K. J. *Inorg. Chim. Acta* **1996**, *250*, 155.
(63) Dattelbaum, D. M.; Omberg, K. M.; Schoonover, J. R.; Martin, R. L.; Meyer, T. J. *Inorg. Chem.* **2002**, *41*, 6071.
(64) O'Regan, B.; Graetzel, M. *Nature* **1991**, *353*, 737.

DOI: 10.1021/ic501682k
Inorg. Chem. 2015, 54, 460−469